YU Kequan (Orcid ID: 0000-0002-8396-4213)

Performance-enhancement of high-strength strain-hardening cementitious composite (HS-SHCC) by nano-particles: Mechanism and property characterization

Yao Ding[1], Kequan Yu[2*], Weihao Mao[1], Shuo Zhang[3]

kequany@umich.edu

1. College of Civil Engineering, Chongqing University, Chongqing, China

2. Department of Civil and Environmental Engineering, University of Michigan, United State

This is the author manuscript accepted for publication and has undergone full peer review but has not been through the copyediting, typesetting, pagination and proofreading process, which may lead to differences between this version and the Version of Record. Please cite this article as doi: 10.1002/suco.202000637

3. Guangzhou Institute of Building Science Co., Ltd., Guangzhou

Abstract

Nano-SiO_2 (NS), due to its prominent nucleation and pozzolanic effects, holds the promise to effectively enhance the tensile and compressive properties of high-strength strain-hardening cementitious composite (HS-SHCC) at both early age (1d, 3d) and normal curing age (28d). The influence of nano-SiO_2 (NS) on the hydration, microstructure and mechanical properties of HS-SHCC with different dosages (i.e., 0, 1, 2, and 3% by mass of cement) were explored in this research. The nucleation effect of NS particles accelerated the hydration process, and the pozzolanic reaction tended to improve the hydration degree of matrix at the micro-scale. The addition of NS particles decreased the porosity and refined the pore structure of the matrix. Single-fiber pullout tests (meso-scale) showed a remarkable improvement of interfacial bond stress with the incorporation of NS particles and consequently on the macro-scale mechanical strengths enhancement of HS-SHCC. The linkage between meso- and macro-scale properties was established based on the micro-mechanical model. The combination of filler effect, acceleration effect and pozzolanic reaction of NS particles enhanced the microstructures and mechanical properties of HS-SHCC. The increase in compressive and tensile strength of NS-modified HS-SHCC could reach to 45% (1d) and 30% (1d), respectively, compared to those values of the reference specimen without NS addition. This research provided an effective way to enhance the tensile performance of HS-SHCC, especially for the early-age tensile property.

Keywords: High-strength strain-hardening cementitious composite; Mechanical properties; Microstructures; Multi-scale; Nano-SiO_2

1 Introduction

Ultra-high performance concrete (UHPC) with extremely low water-to-binder ratio has attracted increasing attention because of its high compressive strength and excellent durability [1]. Nonetheless, it is still challenging for UHPC to achieve an obvious strain-hardening behavior with a strain capacity of larger than 0.5% [2]. Compared to UHPC, strain-hardening cementitious composite (SHCC) could exhibit better ductility whereas less compressive strength [3,4]. Designed according to micro-mechanical, SHCC shows strain-hardening behavior with multiple cracking. Its tensile strain capacity can reach up to 3-5% under the assistance of polyvinyl alcohol (PVA) fibers [5-7] or polyethylene (PE) fibers [8-15]. Recently, the authors have successfully developed a cementitious material featuring both high strength and excellent ductility, combining the advantages of UHPC and SHCC simultaneously [8-10], which is termed as high-strength strain-hardening cementitious composite (HS-SHCC) with compressive strength beyond 100 MPa, tensile strength larger than 15 MPa and tensile strain capacity of 6-10 %.

Over the past two decades, a considerable amount of work has been carried out to introduce fine and ultra-fine materials (nano-sized particles) into cement pastes to clarify their influences on cement properties [16-19]. It has already been known that the fineness of the cementitious particles affects their reactivity with water and in general, a finer particle leads to a more rapid reaction [18]. Nano-particles are added as admixtures or partially replace the cement [17,18]. In either case, the addition of nano-sized particles can not only improve the rheological properties at the fresh state [19,20] but also the compressive strength at the hardened state [21,22]. Among the most commonly used nano-sized particles in cementitious materials such as carbon nano-tube, nano-TiO_2, nano-SiO_2, and nano-Al_2O_3 [16,18,23,24], nano-SiO_2 (NS) presents distinctive performance because of its large specific area and high pozzolanic activity [25,26]. According to previous researches [26,27], the roles of NS can be summarized as follows: (1) NS acts as fillers in concrete, which could enhance the particle packing density and eventually enhance the compressive strength; (2) well distributed NS acts as nucleation agents of hydrated products which increases the hydration rate; (3) the chemical reaction between NS and calcium hydroxide (CH) assists to form the clusters of calcium-silicate-hydrate; (4) the structure of the interfacial transition zones between aggregates and paste, fiber and matrix can be modified with NS addition.

According to previous studies, NS could improve the compressive strength of UHPC at both the early age [28,29] and the normal curing-age (28d) [28-30] due to the above-mentioned effects. As expected, besides the

enhancement on the compressive strength, the influence of NS addition could also increase the tensile properties of UHPC. The frictional stress between the steel fiber and the matrix of UHPC increased with the NS dosage up to an optimal threshold, but the influence of NS particle on the tensile properties including the tensile strength and tensile capacity of UHPC at the composites scale has not been specified [31]. The compressive and flexural properties of nano-modified normal strength SHCC at composites scale has been investigated, while the impact of nano-particle on the frictional stress between the fiber and matrix has not been revealed [32]. It has been known that the macro-mechanical performances of cement-based materials are primarily decided by their micro- and meso-structure characteristics [33]. Additionally, compared to normal strength SHCC, NS particles would exhibit more effectively in the HS-SHCC matrix considering the compatible size of NS particles and the pore size in the HS-SHCC system. Thus, a multi-scale analysis on NS-modified HS-SHCC, especially focusing on promoting the tensile properties at composites level through optimizing its micro- (matrix property) and meso-properties (fiber/matrix interfacial bond), is meaningful and remains to be clarified.

In this paper, the contributions of NS on the performance of HS-SHCC at both early age and normal curing age were investigated. The micro-structure characteristics, compressive strength and tensile properties of HS-SHCC with four different NS contents (i.e., 0, 1, 2 and 3%) at different curing ages (i.e., 1, 3, and 28d) were evaluated. The hydration of matrix, crystalline phases and pore structures were investigated by isothermal calorimetric, thermal gravimetric analysis (TGA) and mercury intrusion porosity (MIP) test, respectively. Single-fiber pullout tests at the meso-scale were conducted to link the micro property and macro tensile properties of HS-SHCC through the micro-mechanical model

2 Experimental Scheme

2.1 Mixture components

The HS-SHCC mixture had four components, i.e., cementitious binder, aggregate, fiber reinforcement and NS particle. The binder materials were P.O. 52.5R, limestone powder (LP), slag and silica fume (SF). The compressive strengths of standard cement mortar samples were 53.2 and 61.9 MPa at 7d and 28d, respectively. LP was used to partially replace the cement amount to reduce the hydration heat, viscosity and increase the matrix flowability. slag and SF were added to promote secondary hydration. The silica sand was used as the aggregate. The particle size distributions of these raw materials increased successively from small to large as SF 0.1-1 μm, LP 1-10 μm, slag 5-100 μm and silica sand (40-180 μm), benefiting the particle packing density and strengthening

the interfaces between the aggregates and paste, the fibers and matrix. The particle size distributions of SF, LP, slag, OPC and fine silica sand could be referred to [8].

A powder polycarboxylate-based superplasticizer (SP) was incorporated to guarantee the flowability of the HS-SHCC matrix. The dosage of SP in the reference sample without NS addition was settled at 10 kg/m^3 for achieving a well-dispersed system. A commercially available NS with an average particle size of 30 nm was used. The morphologies of the NS particles obtained from SEM are shown in Fig. 1. Extremely fine NS particles with some agglomeration were observed.

The length and diameter of PE fiber were 18 mm and 24 μm, respectively, resulting in an aspect ratio L_f/d_f of 750. A higher L_f/d_f ratio could generate a larger fiber/matrix interfacial area [34,35] and improve the fiber-bridging capacity. The tensile strength of PE fiber is 3000 MPa according to the manufacturer.

2.2 Specimens preparation

The mixture proportion of reference HS-SHCC sample without NS incorporation (NS0) was designed according to previous works [8-10] and is illustrated in Table 1. The water-to-binder ratio and the PE fiber volume content were set constant at 0.14 and 2%, respectively. The mixtures with 0, 1, 2, and 3% NS addition by mass of cement, were designated as NS0, NS1, NS2, and NS3, respectively.

The following mixing procedure was performed for all HS-SHCC mixtures. Solid ingredients (e.g. OPC, SF, slag, LP, and sand) were mixed for 1 min at low speed (i.e., 140 rpm). Then, a solution containing tap-water and powder-based SP was slowly added into the dry ingredients and mixed for an additional 5 min at 140 rpm and 1 min at high speed (i.e., 420 rpm). After assuring that the mixtures were adequately workable, NS was added and mixed at 420 rpm for 2 more minutes. At the final stage, PE fiber was gradually added into the fresh mixture and mixed at 140 rpm until uniformly dispersed. After casting and compacting, all specimens were covered with plastic film for 24h at a temperature of 20 ± 2 °C and relative humidity of more than 95%. After that, all the specimens were demolded and cured in a water tank until the planned curing ages (i.e., 3 and 28d).

Flowtable tests were conducted according to Chinese Standard GB2419-2005 (2005) [36] to assure the similar flowability of the fresh HS-SHCC matrix. All the mixtures had a similar flow value of 240 mm via adjusting the SP dosage in NS-modified HS-SHCC mixtures (SP dosages are 10.2, 10.4 and 10.7 g for NS1, NS2, NS3,

respectively).

2.3 Experimental methods

The experiments in this investigation were conducted at three scales. For micro-scale properties, the NS-modified HS-SHCC matrix without PE fiber (i.e., NS0, NS1, NS2, and NS3) at different curing ages (i.e., 1, 3, and 28d) were characterized by hydration kinetics measurement, TG/DTG and MIP tests. The detailed experimental descriptions could be referred to [9]. At the meso-scale, ten samples of each mixture were prepared for single-fiber pullout tests at 1d and 28d, and the test set-up is shown in Fig. 2a. For macro-scale properties, the compressive strengths of HS-SHCC containing different NS dosages (i.e., 0-3%) at the ages of 1, 3, and 28d were tested by using five 50 mm cubes (ASTM 2013 [37]). The corresponding tensile performances of HS-SHCC mixtures were measured by using dogbone specimens (JSCE 2008 [38]) under uniaxial tensile tests (Fig. 2b). The detailed testing scheme is listed in Table 2. Further testing descriptions for meso- and macro- scales could be referred to [9].

3 Experimental outputs and Discussion

3.1 Hydration kinetics

Figure 3a indicates the effect of NS dosages on the hydration heat evolution of the HS-SHCC matrix in the first 48h. A period of rapid hydration heat evolution occurred immediately when mixed with water (stage 1) due to the initial dissolution of ions. Then, the hydration heat evolution rate decreased rapidly and entered in an inactive period called dormant stage (stage 2), in which the concentration of Ca^{2+} reached a saturated state. Stage 3 began by the end of the dormant period and associated with the main heat peak. In this period, active components such as C_3S began to react again and silicate continued to hydrate rapidly. The reaction rate afterwards slowed down until a stable state was achieved (stage 4). The incorporation of NS reduced the dormant period and advanced the appearance of the second heat peak. As can be seen in Fig. 3a, the dormant period of NS0 was about 10h, whereas this period was reduced to around 6h with NS addition. This might be due to the seeding and the chemical effects deduced by NS. It is known that the rate of hydration is mainly decided by the surface area of nano-particles. NS particles with the high surface area could accelerate hydration, and thus high hydration heat was obtained (Zyganitidis et al. 2011). Further, the pozzolanic reaction of NS with CH could also benefit the hydration process. Nevertheless, it is worth noticing that the NS2 matrix had a higher hydration heat than that of the NS3. This could

be caused by that excessive nano-sized particles could not be dispersed properly and generated a negative influence on the heat evolution rate [17].

Figure 3b illustrates the cumulative heat normalized by unit cementitious material. In general, the addition of NS particles increased the unit heat release compared to that of the reference mixture (NS0). The NS2 matrix exhibited the largest cumulative heat release because of the chemical reaction and the nucleation effect of NS particles, yet higher NS content up to 3% could not further induce a positive influence on hydration.

3.2. TG/DTG analysis

Figure 4 plots the TG/DTG curves of HS-SHCC matrices at 28 d. As shown in Fig. 4a, there are three primary weight losses in the TG curves. The first weight loss corresponded to the evaporation of water. With the rise of temperature to around 450°C, the dehydroxylation of CH occurred and calciumoxide formed. Due to the decarbonisation of $CaCO_3$ accompanied by CO_2 escaping at around 650°C, the third weight loss was generated. Referring to the DTG curves (see in Fig. 4b), the intensity of the third endothermal peak which was mainly caused by the decomposition of limestone powder (LP) introduced from raw materials was almost the same for all the four HS-SHCC matrices.

Figure 5 presents the TG/DTG curves of NS2 matrices at the age of 1, 3 and 28d. It is clear from Fig. 5a that the weight losses for the sample at 28d were greater than those at 1d and 3d since the amount of hydrated product increased with the increase of hydration time. Moreover, as shown in Fig. 5b, it is obvious that the AFt peak was weakened whereas the intensity of the C-S-H peak was notably strengthened as the curing age was prolonged. This suggests the optimization of microstructures with curing time and the development of strength.

The degree of hydration with time can be reflected by the CH content in the HS-SHCC matrix (ranging from 380 °C and 450 °C). The relative amounts of CH formed in the HS-SHCC matrix with age are shown in Fig. 6. The CH amount in HS-SHCC matrix with NS addition is balanced by two factors: (i) NS particles acting as nucleation agents of hydrated products accelerate hydration rate, which releases more CH; (ii) the pozzolanic activity of NS consumes CH to form C-S-H. As shown in Fig. 6, the relative CH amounts of NS-modified matrices were higher than that of the control sample at 1d due to that the seeding effect could control the amount of CH in the early period, and the matrix with 2% NS incorporation generated the highest amount of CH. Adversely, a remarkably lower CH content was observed in the NS-modified matrix especially for NS2 at 3d and 28d than that of NS0. This might be caused by that the amount of CH consumed by the pozzolanic reaction of NS

surpassed that released from hydration. No matter which effect was the dominant one, NS inclusion benefited the development of strength because more C-S-H gels formed, especially at an early age. The detailed information of mechanical properties is analyzed in Sections 3.5 and 3.6.

3.3 Porosity and pore size distribution

The pore structure, including the porosity and pore size distribution, of NS0 and NS2 at different curing ages, are shown in Fig. 7. As expected (see in Fig. 7a), the total porosity reduced significantly with increasing curing age for continued hydration regardless of NS particle. The porosity of NS2 specimens decreased from 16.5% to 1.78% when the curing age was prolonged from 1d to 28d. Moreover, the dv/dlog(d) curves (see in Fig. 7b) shifted to the left and the peak value demonstrating the critical pore size reduced with curing age. All these results coincided well with the considerable strength improvement with curing age stated in the following sections.

It could be observed from Fig. 7a that regardless of curing age, the incorporation of NS with 2% addition reduced the porosity. For example, the porosity at 28d decreased from 2.16% to 1.78% with a 17.6% decrease when NS was incorporated. Additionally, as shown in Fig. 7b, the curves for NS2 moved to the left when the pore sizes were less than 40 nm at 1d and 20 nm at 3d, respectively, representing more pores with smaller size existed in NS-modified HS-SHCC matrix. Moreover, the peak value of the dv/dlog(d) curve for NS2 was lower than that of NS0. These above results indicate that the incorporation of NS with 2% content significantly decreased the total porosity and refined the pores, resulting in a denser and more homogeneous HS-SHCC, especially at the early age. Furthermore, no obvious peaks were observed on the dv/dlog(d) curves in the ranges of micro-pores (<10 nm) and meso-pores (10-50 nm), demonstrating a high strength of HS-SHCC at 28d.

3.4 Single-fiber pullout test

The load-displacement curves obtained from single-fiber pullout tests are shown in Fig. 8, and most of the fibers were pulled out from the matrix. The load decreased obviously onset of fiber debonding followed by a subsequent increase, exhibiting the slip-hardening behavior (Fig. 8c) which was the basis of the macro-scale strain-hardening behavior.

Figure 9a shows the interfacial bond stress at different NS dosages. The average interfacial bond stress (calculated by Eq. 1) increased with the increasing NS content until the NS content surpassed 2% with the average values of 1.38, 1.53, 1.62 and 1.42 MPa for NS0, NS1, NS3 and NS4 at 28d, respectively. As can be seen in Fig. 9b, the interfacial bond stress also increased obviously as curing age increased from 1d to 28d. As stated in Section 3.3,

the reduction of porosity and the refinement of the pore size distribution led to the improvement of interfacial bond stress with NS addition and curing age. Further, the increased interfacial bond stress would generate a higher tensile strength at the macro-scale (Section 3.6).

$$\tau_0 = \frac{F}{\pi d_f l_{em}} \quad (1)$$

where F is the peak force and l_{em} is the embedded fiber length.

3.5 Compressive property

The effects of NS dosage on the compressive strength of HS-SHCC at different curing ages are demonstrated in Fig. 10. The incorporation of NS promoted the compressive strength of HS-SHCC for all ages with an optimal NS content at 2%. The 28d compressive strength of reference HS-SHCC NS0 was 127.5 MPa and the compressive strength of NS2 was 16.2% larger than that of the control sample (NS0). Nevertheless, when the NS content was further improved to 3%, the improvement of compressive strength decreased to 7.6% because an overdose of nanoparticles could lead to agglomerate and result in voids and weak zones formation [17]. The strength improvement could be mainly attributed to the following three positive effects of NS in cement paste. (i) The physical filler effect of NS particles could generate a denser matrix with lower porosity which benefits the strength enhancement of cement paste in the hardened state (referring to Section 3.3). (ii) The hydration rate would be accelerated by the addition of NS as mentioned in Section 3.1, generating more C-S-H which contributes critically to strength development. (iii) The pozzolanic activity of NS consuming CH to form additional C-S-H, which refines the pore structure and leads to a denser microstructure (referring to Sections 3.2 and 3.3), could further benefit the strength development.

Figure 10 also indicates that the compressive strength of HS-SHCC enhanced with curing age. The highest rate of strength gain happened between 1d and 3d for all the mixtures. The 3d compressive strength of HS-SHCC without NS modification (i.e., 108.7 MPa) surpassed its 1d compressive strength (i.e., 46.1 MPa) by 135.8%. Between 7d and 28d, the rate of strength gain significantly decreased for all the mixtures, and the 28d compressive strength of the control sample (i.e., 127.5 MPa) was 17.3% higher than its 3d strength. As the compressive strengths were normalized to those of the control sample (NS0) at 1, 3, and 28d, respectively, it is clear that the enhancement of compressive strength of NS-modified HS-SHCC was most obvious at 1d for all mixtures as shown in Fig. 10b.

When the dosage of NS was 2%, its 1d compressive strength (i.e., 66.3 MPa) was 43.7% higher than that of the control sample; whereas its 3d and 28d strength values were 16.8% and 16.2% greater compared to the control sample, respectively. This might be due to that the hydration rate was evidently accelerated by the addition of NS especially at the early age with the NS content of 2% as mentioned in Section 3.1, and thus the early formed C-S-H would develop a higher compressive strength at 1d.

3.6 Tensile performance

3.6.1 Stress-strain curves

The tensile stress-strain relationship of NS-modified HS-SHCC at 28d are presented in Fig. 11. All these specimens presented a robust strain-hardening performance. Every stress reduction in the strain-hardening process corresponded to the formation of a new crack.

Moreover, the influence of curing age on the average stress-strain cures of HS-SHCC is summarized in Fig. 12. It is clear that even at early ages (e.g., 1d and 3d, see in Fig. 12a and b), HS-SHCC specimens with or without NS modification all featured with strain-hardening performance. In general, the peak stress increased while the strain capacity decreased with the increase of curing age as shown in Fig. 12d. For instance, the peak stress of NS2 increased from 10.8 MPa to 15.0 MPa with a 38.9% increase while the strain capacity exhibited a 31.4% reduction as the curing age increased from 1d to 28d.

The cracking patterns of HS-SHCC with NS dosage of 2% after unloading at different ages are summarized in Fig. 13. It is noted that multiple cracks saturated over the gauge length and no localized cracks were observed under high imposed strain level regardless of the curing age. The specific values of crack numbers and residual crack widths can be found in Fig. 15.

3.6.2 Tensile parameters

The tensile parameters of HS-SHCC included the mechanical and crack pattern parameters. The mechanical parameter consisted of the initial cracking stress, peak stress, corresponding strain capacity and strain energy density under the area between the stress-strain curve and *X*-axis. Crack pattern parameter included the crack numbers, crack spacing and average crack widths.

The influences of NS dosage, as well as curing age on the tensile parameters of HS-SHCC, are summarized and

compared in Fig. 14. As expected (Fig. 14a), the peak stress grew with the increasing curing age regardless of the existence of the NS particles. Compared with the peak stress of NS2 at 1d (i.e., 10.3 MPa), this value increased by 32.4% and 61.2% when the curing age was prolonged to 3d and 28d, respectively. The incorporation of NS increased the peak stress in an optimal dosage range of 1-2%. For instance, as the dosage of NS increased from 1% to 2%, the peak stress of HS-SHCC at 28d improved from 15.0 MPa to 17.1 MPa with 4.2% and 18.8% increase, respectively, compared to that of the reference sample (NS0). Further improvement of NS content to 3% generated a slight effect on the improvement of peak stress of HS-SHCC regardless of the curing age. The aforementioned positive effects of NS, including physical filling effect, acceleration effect, and pozzolanic effect could notably increase the packing density and refine the pore structure, resulting in higher tensile strength of the composites. Additionally, the enhanced interfacial friction strength between PE fiber and NS-modified matrix as illustrated in Section 3.4 would further improve the tensile strength of HS-SHCC. Similarly, it is clear from Fig. 14b that the initial cracking stress also increased with curing age, and its value reached 11.8 MPa for NS-28d specimen.

From Fig. 14a and c, it is clear that the improvement in strength always accompanied by the sacrifice of strain capacity. Referring to NS2, which owned the highest peak stress (i.e., 17.1 MPa) exhibited the lowest strain capacity (i.e., 6.03%) at 28d. Additionally, the strain capacity of all HS-SHCC specimens decreased with the extending of curing age (see in Fig. 14c). The 1d strain capacity of NS2 was 8.62%, then, this value decreased to 8.35% at 3d and further decreased to 6.03% at 28d. Both phenomena were caused by the increase of compressive strength and thus the increase of matrix toughness, which generated adverse influence on tensile ductility. Wu [40] stated that a certain range of interface friction strength was required for a certain matrix toughness in order to obtain steady-state crack condition. It is known that fiber pullout facilitates when the interface friction strength is below the minimum value, whereas fiber ruptures as interface friction strength are above the maximum value and both result in premature failure. As the interfacial friction strength reaches the lower limit of the target zone, more fibers are pulled out with a weak slip hardening. Oppositely, when the upper limit of the zone is reached, slip hardening is enhanced, whereas the percentage of fiber rupture before entirely pulled out would increase. Consequently, NS particles added in this study are believed to generate a higher value of interfacial bond strength, which would lead to more fiber rupture in NS-modified samples than that in the control samples (NS0) and thus result in higher tensile strength whereas lower ductility.

The relationships between the strain energy density and NS content at different curing ages are shown in Fig. 14d. It is known that strain energy density is influenced by both strength and ductility. As expected, the strain energy density increased with the prolonging of curing age in general. Additionally, the strain energy density decreased from 942.1 kJ/m^3 (NS0) to 868.1 kJ/m^3 (NS2) at 28d. It is known that fiber pullout would consume more energy than fiber rupture during the pullout process. As discussed above, the addition of 2% NS dosage increased the fiber/matrix interfacial friction strength which caused more fiber rupture compared to that of NS0.

The crack numbers of all HS-SHCC samples were greater than 40 at 28d (Fig. 15). The crack width decreased as curing age prolonged which was consistent with that of the strain capacity, indicating a reduction of ductility with curing age. The average self-controlled residual crack widths of HS-SHCC at 28d were smaller than 150 μm, indicating excellent durability according to ACI 224R [41].

The larger interfacial bond strength between PE fibers and NS-modified matrix has already been demonstrated by single-fiber pullout tests as introduced in Section 3.4, which can be further verified by comparing the fiber failure modes on the fracture surfaces of NS0 and NS2 (Fig. 16). Most of the fibers were pulled out from the NS0 matrix with a fiber pull-out length of around 6-8 mm and the fiber surfaces were relatively smooth (Fig. 16a). However, as presented in Fig. 16b, it is clear that a considerable percentage of fibers ruptured with a much smaller fiber pullout length (i.e., about 2-3 mm) of NS2 compared to that of NS0. The fracture of PE fiber also meant a full utilization of fiber strength capacity in the NS-modified matrix.

3.7 Linkage of meso- and macro-scale properties

Based on the micro-mechanical model, the peak stress of HS-SHCC (σ_{tu}) coincides with the maximum bridging stress (σ_0), given by Lin and Li [34] as follows:

$$\sigma_{tu} = g\sigma_0 \tag{2}$$

$$\sigma_0 = \frac{1}{2}\tau\frac{L_f}{d_f}V_f \tag{3}$$

where g is the snubbing factor of PE fiber [34] and its detailed value can be found in Ref. [42]; τ is the interfacial bond strength; L_f, d_f and V_f are the length, diameter and fiber volume content of PE fiber, respectively. Interestingly, it can be found from Eqs. (2-3) that the peak strength (σ_{tu}) of HS-SHCC at the macro-scale is

linearly dependent on the interfacial bond stress (τ) at meso-scale. The values of experimental tensile strength are compared with the theoretical ones in Fig. 17, demonstrating a good agreement between these two values.

Moreover, the relationship between the crack opening displacement (δ_0) corresponding to the maximum fiber bridging stress (σ_0) and the interfacial bond stress (τ) could be calculated by using Eqs. (4-5) [34,43]:

$$\delta_0 = \frac{\tau L_f^2}{E_f d_f (1+\eta)} \quad (4)$$

$$\eta = V_f E_f / V_m E_m \quad (5)$$

where E_f and V_m are the elastic modulus of PE fiber and fiber volume content; similarly, E_m and V_m are the elastic modulus and the volume of the matrix. For that the volume of PE fiber is extremely small, the value of η is approximated as 0. A linear correlation was found between δ_0 and τ, benefiting the development of strain capacity of HS-SHCC. However, fibers would be more inclined to fracture during the pullout process for NS-modified HS-SHCC, which may adversely affect the development of crack opening and then decrease the strain capacity. In Fig. 14c, the strain capacity of NS2 at 28d was the lowest as well as the crack width as shown in Fig. 15.

4. Conclusions

In this research, the influences of nano-SiO_2 (NS) dosage and curing age on the microstructures and mechanical performance of high-strength strain-hardening cementitious composite (HS-SHCC) were investigated and the conclusions are listed as follows.

(1) At the micro-scale, NS particles accelerated the matrix hydration, reduced the dormant period and advanced the second peak due to the seeding and pozzolanic reaction of NS particle. According to TG/DTG analysis, the C-S-H peak was strengthened as curing age prolonged and CH content decreased, suggesting the optimization of micro-structures and the development of strength with increasing curing age. It is noteworthy that NS particles played different critical roles as the nucleation effect in the early age (1d) and pozzolanic effect in the prolonged curing age (3d, 28d). Besides, NS particles reduced the total porosity and refined the pore structure of HS-SHCC matrix especially at the early age, which consequently induced the positive effect on the mechanical performance development of NS-modified HS-SHCC.

(2) At the meso-scale, the incorporation of NS particles endowed a larger interfacial bond strength between PE

fiber and HS-SHCC matrix. PE fibers ruptured during the pullout process, which meant a full utilization of the tensile strength of fiber, yet a potentially negative effect on the strain capacity. The relationship between the meso- and macro-scale properties was established based on the micro-mechanical model.

(3) At the macro-scale, NS particle benefited the compressive strength of HS-SHCC due to its physical and chemical advantages, but with an optimal content at 2%. The improvement of compressive strength of NS-modified HS-SHCC was most obvious at 1d, which was attributed to the accelerated hydration rate and thus the more early-formed C-S-H gels. The NS particle endowed the HS-SHCC a high-early strength characteristic.

(4) The tensile performance of HS-SHCC were influenced by the dosage of NS as well as the curing age. The addition of NS particles and the prolonged curing age both benefited the tensile strength while exhibited adverse influence on the strain capacity at the macro-scale. The tensile performance of HS-SHCC at composites level was closely linked with and affirmed by those properties obtained at the micro- and meso- scales. According to the discussion in this research, it is an effective method to optimize the mechanical performance of HS-SHCCs at composites level by altering their down-scale properties.

The data that support the findings of this study are available from the corresponding author upon reasonable request.

References

[1] Graybeal, B., & Davis, M. (2008). Cylinder or cube: strength testing of 80 to 200 MPa (11.6 to 29 ksi) ultra-high-performance fiber-reinforced concrete. *ACI Materials Journal*, *105*(6), 603.

[2] Wille, K., El-Tawil, S., & Naaman, A. E. (2014). Properties of strain hardening ultra high performance fiber reinforced concrete (UHP-FRC) under direct tensile loading. *Cement and Concrete Composites*, *48*, 53-66.

[3] Li, V. C. (2003). On engineered cementitious composites (SHCC). *Journal of advanced concrete technology*, *1*(3), 215-230.

[4] Zhang, D., Yu, J., Wu, H., Jaworska, B., Ellis, B. R., & Li, V. C. (2020). Discontinuous micro-fibers as intrinsic reinforcement for ductile Engineered Cementitious Composites (SHCC). Composites Part B: Engineering, 107741.

[5] Liu, J. C., Tan, K. H., & Zhang, D. (2017). Multi-response optimization of post-fire performance of strain hardening cementitious composite. *Cement and Concrete Composites*, *80*, 80-90.

[6] Zhang, Z., & Zhang, Q. (2018). Matrix tailoring of engineered cementitious composites (SHCC) with non-oil-coated, low tensile strength PVA fiber. *Construction and Building Materials*, 161, 420-431.

[7] Meng, D., Huang, T., Zhang, Y. X., & Lee, C. K. (2017). Mechanical behaviour of a polyvinyl alcohol fibre reinforced engineered cementitious composite (PVA-ECC) using local ingredients. *Construction and Building Materials*, 141, 259-270.

[8] Ding, Y., Yu, J. T., Yu, K. Q., & Xu, S. L. (2018). Basic mechanical properties of ultra-high ductility cementitious composites: From 40 MPa to 120 MPa. *Composite Structures, 185*, 634-645.

[9] Ding, Y., Liu, J. P., & Bai, Y. L. (2020a). Linkage of multi-scale performances of nano-$CaCO_3$ modified ultra-high performance engineered cementitious composites (HS-SHCC). *Construction and Building Materials, 234*, 117418.

[10] Ding, Y., Yu, K. Q., & Mao, W. H. (2020b). Compressive performance of all-grade engineered cementitious composites: Experiment and theoretical model. *Construction and Building Materials, 244*.

[11] Li, L.Z., Bai, Y., Yu, K. Q., Yu, J. T., & Lu, Z. D. (2019a). Reinforced high-strength engineered cementitious composite (SHCC) columns under SHCCentric compression: experiment and theoretical model. *Engineering Structures, 198*, 109541.

[12] Li, L.Z, Cai, Z.W, Yu, K.Q, Zhang, Y. X., & Ding, Y. (2019b). Performance-based design of all-grade strain hardening cementitious composites with compressive strengths from 40 MPa to 120 MPa. *Cement and Concrete Composites*, *97*, 202-217.

[13] Lu, Z., Yin, R., Yao, J., & Leung, C. K. (2019). Surface modification of polyethylene fiber by ozonation and its influence on the mechanical properties of Strain-Hardening Cementitious Composites. *Composites Part B: Engineering, 177*, 107446.

[14] Ranade, R., Li, V. C., Stults, M. D., Heard, W. F., & Rushing, T. S. (2013a). Composite Properties of High-Strength, High-Ductility Concrete. *ACI Materials Journal*, *110*(4).

[15] Yu, K. Q., Ding, Y., Liu, J. P., & Bai. Y. L. (2020). Energy dissipation characteristics of all-grade polyethylene fiber-reinforced engineered cementitious composites (PE-SHCC). *Cement and Concrete Composites*, 106.

[16] Chen, J., Kou, S. C., & Poon, C. S. (2012). Hydration and properties of nano-TiO2 blended cement composites. *Cement and Concrete Composites*, *34*(5), 642-649.

[17] Li, H., Xiao, H. G., Yuan, J., & Ou, J. (2004). Microstructure of cement mortar with nano-particles. *Composites Part B: Engineering*, *35*(2), 185-189.

[18] Jo, B. W., Kim, C. H., Tae, G. H., & Park, J. B. (2007). Characteristics of cement mortar with nano-SiO2 particles. *Construction and building materials, 21*(6), 1351-1355.

[19] Senff, L., Labrincha, J. A., Ferreira, V. M., Hotza, D., & Repette, W. L. (2009). Effect of nano-silica on rheology and fresh properties of cement pastes and mortars. *Construction and Building Materials, 23*(7), 2487-2491.

[20] Senff, L., Hotza, D., Repette, W. L., Ferreira, V. M., & Labrincha, J. A. (2010). Mortars with nano-SiO2 and

micro-SiO2 investigated by experimental design. *Construction and Building Materials*, *24*(8), 1432-1437.

[21] Haruehansapong, S., Pulngern, T., & Chucheepsakul, S. (2014). Effect of the particle size of nanosilica on the compressive strength and the optimum replacement content of cement mortar containing nano-SiO2. *Construction and Building Materials*, *50*, 471-477.

[22] Qing, Y., Zenan, Z., Deyu, K., & Rongshen, C. (2007). Influence of nano-SiO2 addition on properties of hardened cement paste as compared with silica fume. *Construction and building materials*, *21*(3), 539-545.

[23] Nazari, A., Riahi, S., Riahi, S., Shamekhi, S. F., & Khademno, A. (2010). Influence of Al_2O_3 nanoparticles on the compressive strength and workability of blended concrete. *Journal of American Science*, *6*(5), 6-9.

[24] Siddique, R., & Mehta, A. (2014). Effect of carbon nanotubes on properties of cement mortars. *Construction and Building Materials*, *50*, 116-129.

[25] Sanchez, F., & Sobolev, K. (2010). Nanotechnology in concrete–a review. *Construction and building materials*, *24*(11), 2060-2071.

[26] Sobolev, K., & Gutiérrez, M. F. (2005). How nanotechnology can change the concrete world. *American Ceramic Society Bulletin*, *84*(10), 14.

[27] Sobolev, K., Flores, I., Torres-Martinez, L. M., Valdez, P. L., Zarazua, E., & Cuellar, E. L. (2009). Engineering of SiO 2 nanoparticles for optimal performance in nano cement-based materials. In *Nanotechnology in construction 3* (pp. 139-148). Springer, Berlin, Heidelberg.

[28] Rong, Z., Sun, W., Xiao, H., & Jiang, G. (2015). Effects of nano-SiO2 particles on the mechanical and microstructural properties of ultra-high performance cementitious composites. *Cement and Concrete Composites*, *56*, 25-31.

[29] Wu, Z., Shi, C., Khayat, K. H., & Wan, S. (2016). Effects of different nanomaterials on hardening and performance of ultra-high strength concrete (UHSC). *Cement and Concrete Composites*, *70*, 24-34.

[30] Li, W., Huang, Z., Cao, F., Sun, Z., & Shah, S. P. (2015). Effects of nano-silica and nano-limestone on flowability and mechanical properties of the ultra-high-performance concrete matrix. *Construction and Building Materials*, *95*, 366-374.

[31] Wu, Z., Khayat, K. H., & Shi, C. (2017). Effect of nano-SiO_2 particles and curing time on development of fiber-matrix bond properties and microstructure of ultra-high strength concrete. *Cement and Concrete Research*, *95*, 247-256.

[32] Yeşilmen, S., Al-Najjar, Y., Balav, M. H., Şahmaran, M., Yıldırım, G., & Lachemi, M. (2015). Nano-modification to improve the ductility of cementitious composites. *Cement and Concrete Research*, *76*, 170-179.

[33] Sorelli, L., Constantinides, G., Ulm, F. J., & Toutlemonde, F. (2008). The nano-mechanical signature of ultra-high performance concrete by statistical nanoindentation techniques. *Cement and Concrete Research*, *38*(12), 1447-1456.

[34] Lin, Z., & Li, V. C. (1997). Crack bridging in fiber reinforced cementitious composites with slip-hardening interfaces. *Journal of the Mechanics and Physics of Solids*, *45*(5), 763-787.

[35] Naaman, A. E., & Najm, H. (1991). Bond-slip mechanisms of steel fibers in concrete. *Materials Journal*, *88*(2), 135-145.

[36] Chinese National Standard (2005). Test Methods for Flowability of Cement Paste, *GB2419–2005*.

[37] ASTM, C. (2013). Standard test method for compressive strength of hydraulic cement mortars (using 2-in. or [50-mm] cube specimens). *Annual Book of ASTM Standards Annual Book of ASTM Standards*, *4*(1), 1-9.

[38] JSCE. 2008. Recommendations for Design and Construction of High-Performance Fiber Reinforced Cement Composites with Multiple Fine Cracks. Japan Society of Civil Engineers, Tokyo, Japan, pp. 1-16.

[39] Zyganitidis, I., Stefanidou, M., Kalfagiannis, N., & Logothetidis, S. (2011). Nanomechanical characterization of cement-based pastes enriched with SiO2 nanoparticles. *Materials Science and Engineering: B*, *176*(19), 1580-1584.

[40] Wu, C. (2001). *Micromechanical tailoring of PVA-SHCC for structural applications* (Doctoral dissertation), University of Michigan, 2005.

[41] American Concrete Institute, & ACI Committee 224. (2001). *Control of Cracking in Concrete Structures-ACI 224R-01*. American Concrete Institute-ACI.

[42] Ranade R, Li V C, Stults, M D, Rushing T S, Roth J, Heard W F. (2013b). Micromechanics of high-strength, high-ductility concrete. *ACI Materials Journal*, *110*(4), 375-384.

[43] Li, V. C., Mishra, D.K., & Wu, H.C. (1995). Matrix design for pseudo-strain-hardening fibre reinforced cementitious composites. *Materials and Structures*, *28* (10), 586–595.

Table 1 Mixture proportion of HS-SHCC without NS (NS0)

Cement (OPC) (kg/m^3)	Limestone powder (LP) (kg/m^3)	Silica fume (SF) (kg/m^3)	slag (kg/m^3)	Silica sand (kg/m^3)	Water (W) (kg/m^3)	PE fiber (kg/m^3)	SP (kg/m^3)	W/B
700	100	150	750	500	230	20	10	0.14

Table 2 Test scheme of NS-modified HS-SHCC

Mix proportions	Curing age	Number of specimens				
		TG/DTG	MIP	Single-fiber pullout	Compression	Tension
NS0, NS1, NS2, and NS3	1d, 3d, 28d	1	1 (NS0 &NS2)	10	5	4

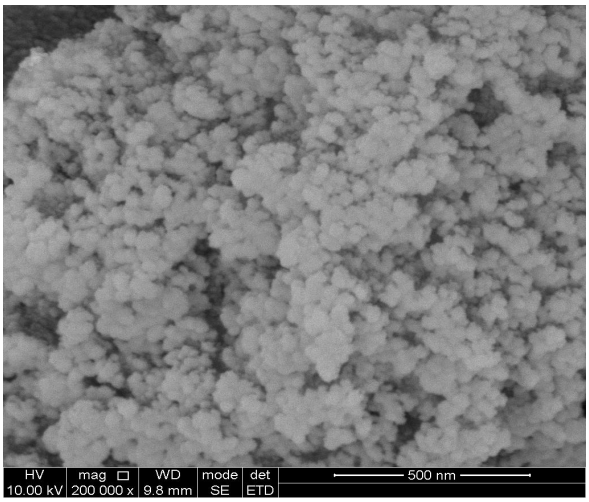

Fig. 1 Morphology of NS particles

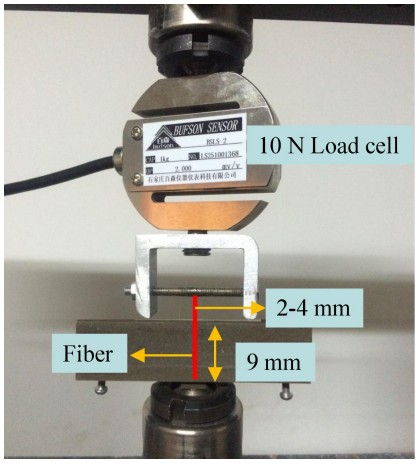

(a) Single-fiber pullout test

(b) Uniaxial tensile test

Fig. 2 Test setups

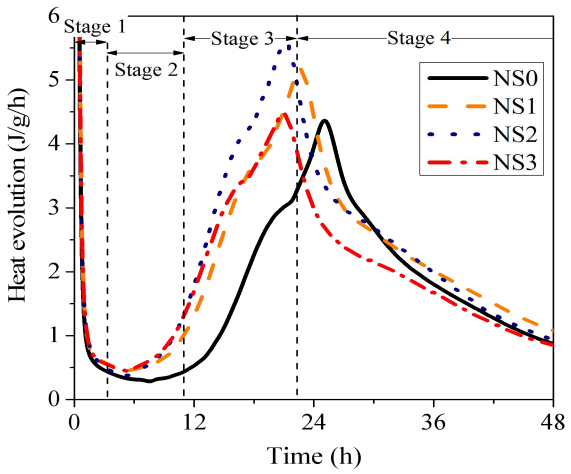

(a) Hydration heat evolution rate

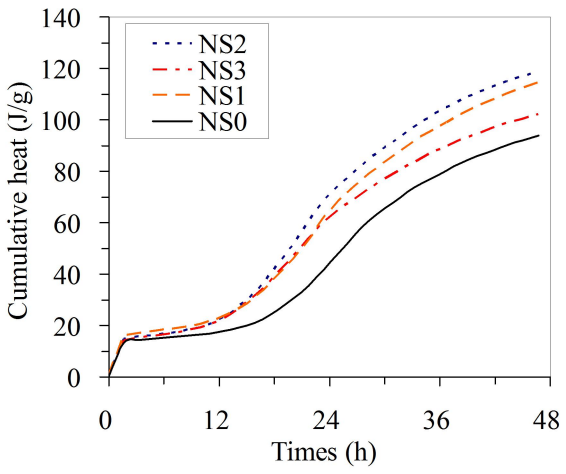

(b) Heat release normalized by unit cementitious material

Fig. 3 Hydration evolution of HS-SHCC matrices

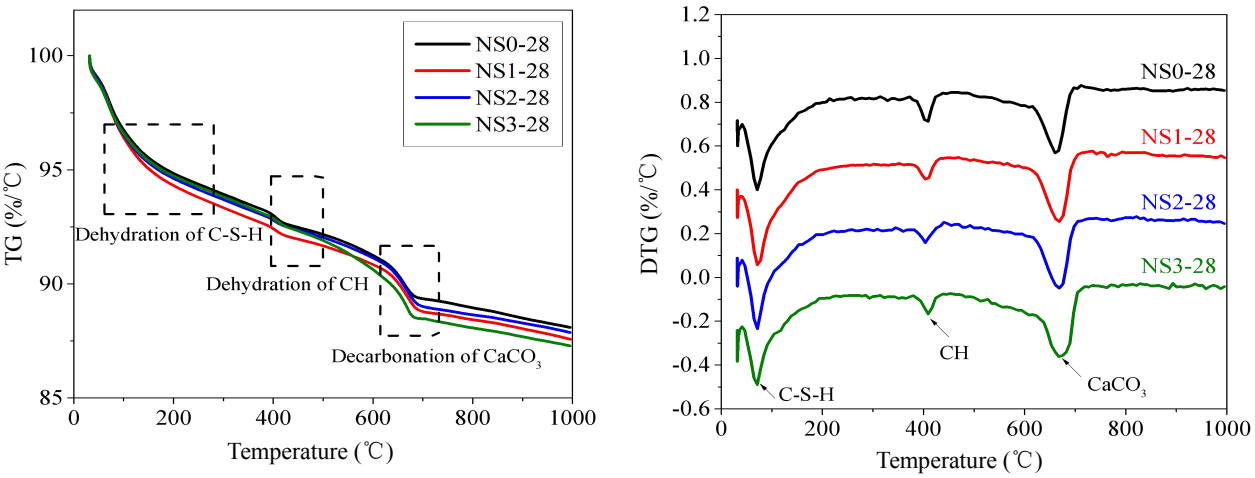

(a) TG curves (b) DTG curves

Fig. 4 Matrix TG/DTG curves with different NS contents at 28d

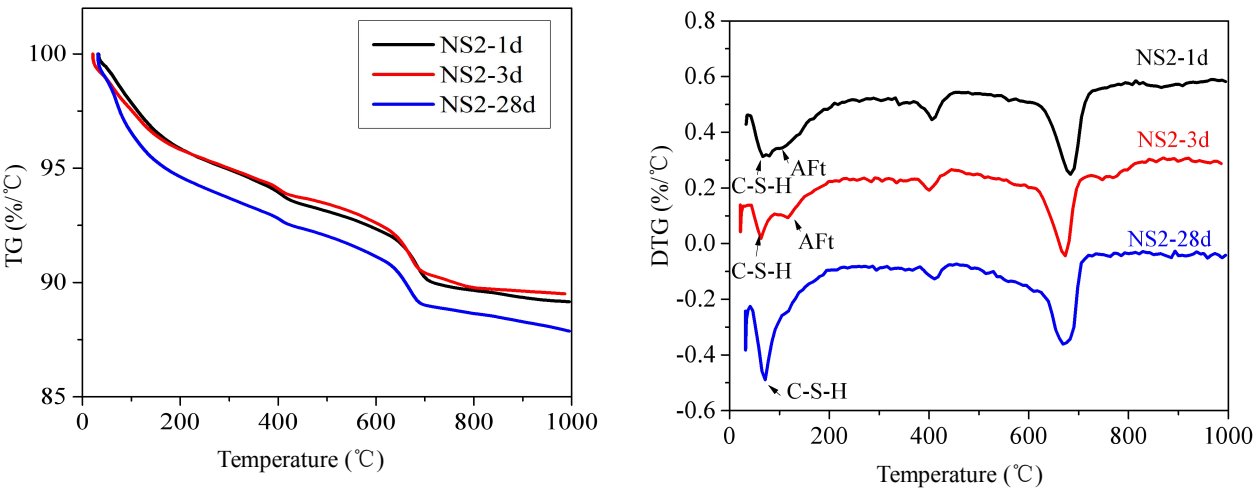

(a) TG curves (b) DTG curves

Fig. 5 TG and DTG curves of NS2 at different ages

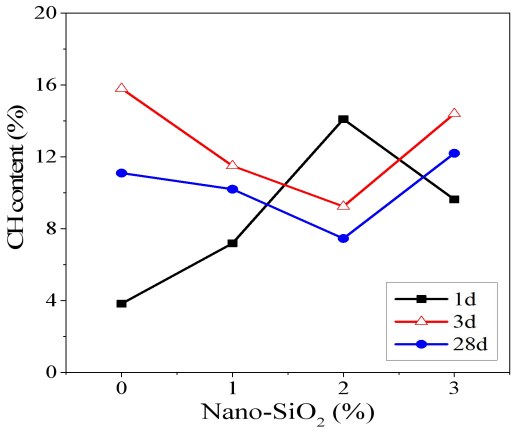

Fig. 6 Amount of CH formed in HS-SHCC samples at different ages

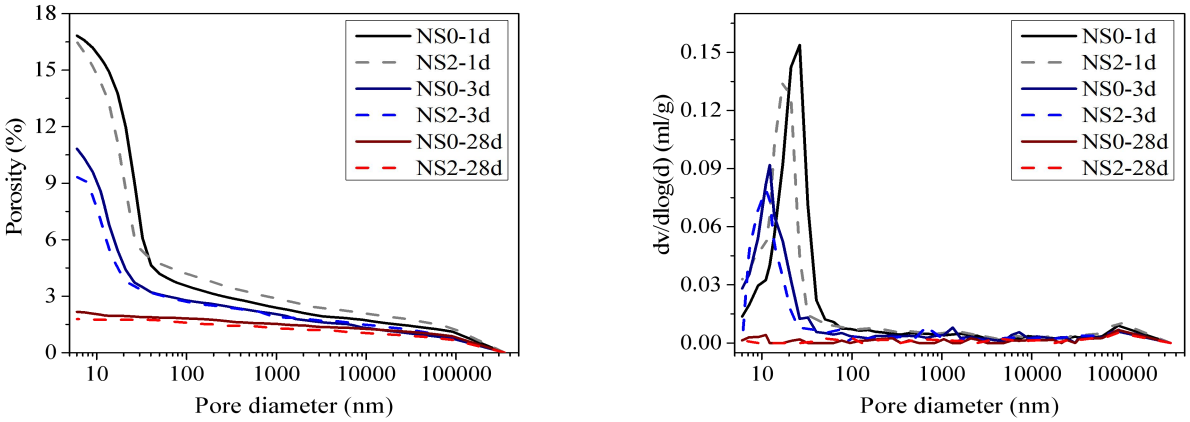

(a) Porosity (b) Pore size distribution

Fig. 7 Porosity properties of NS-modified HS-SHCC

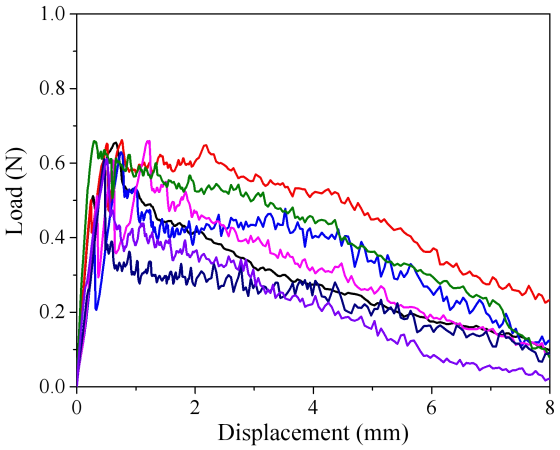

(a) NS2-1d

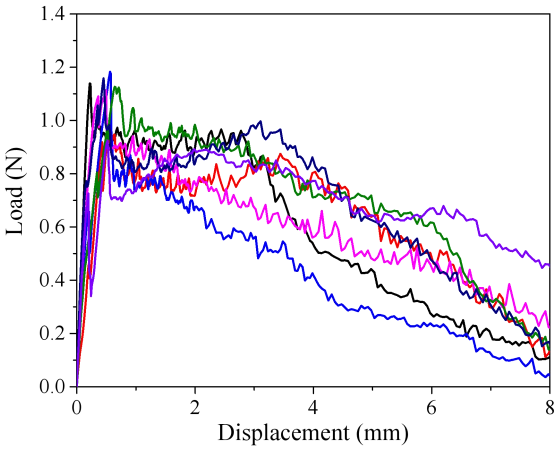

(b) NS2-28d

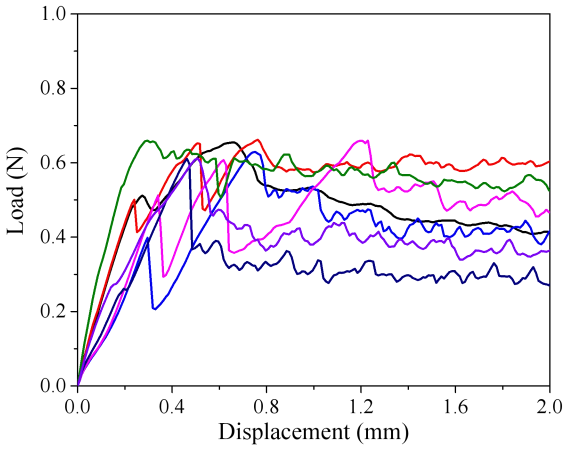

(c) Partially enlarged curves of NS2-1d

Fig. 8 Single-fiber pullout test results

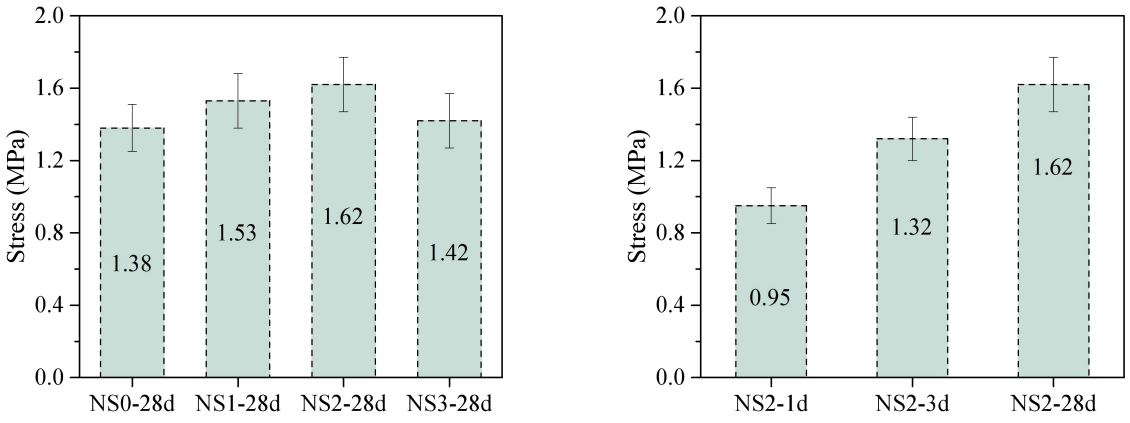

(a) NS content (b) Curing age

Fig. 9 Effect of NS content and curing age on interfacial bond stress of HS-SHCC

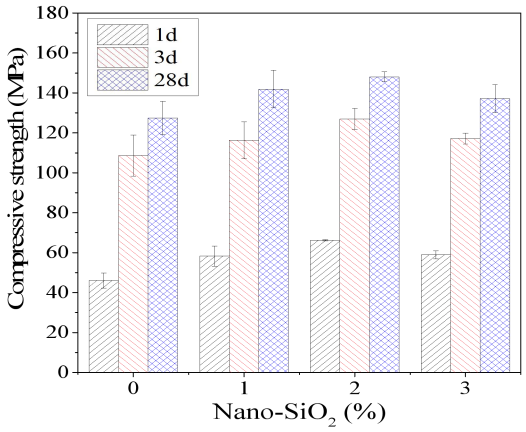

(a) Compressive strength

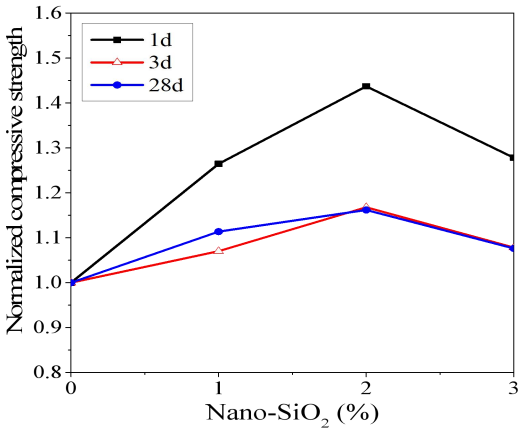

(b) Normalized compressive strength

Fig. 10 Effect of NS content and curing age on compressive strength of HS-SHCC

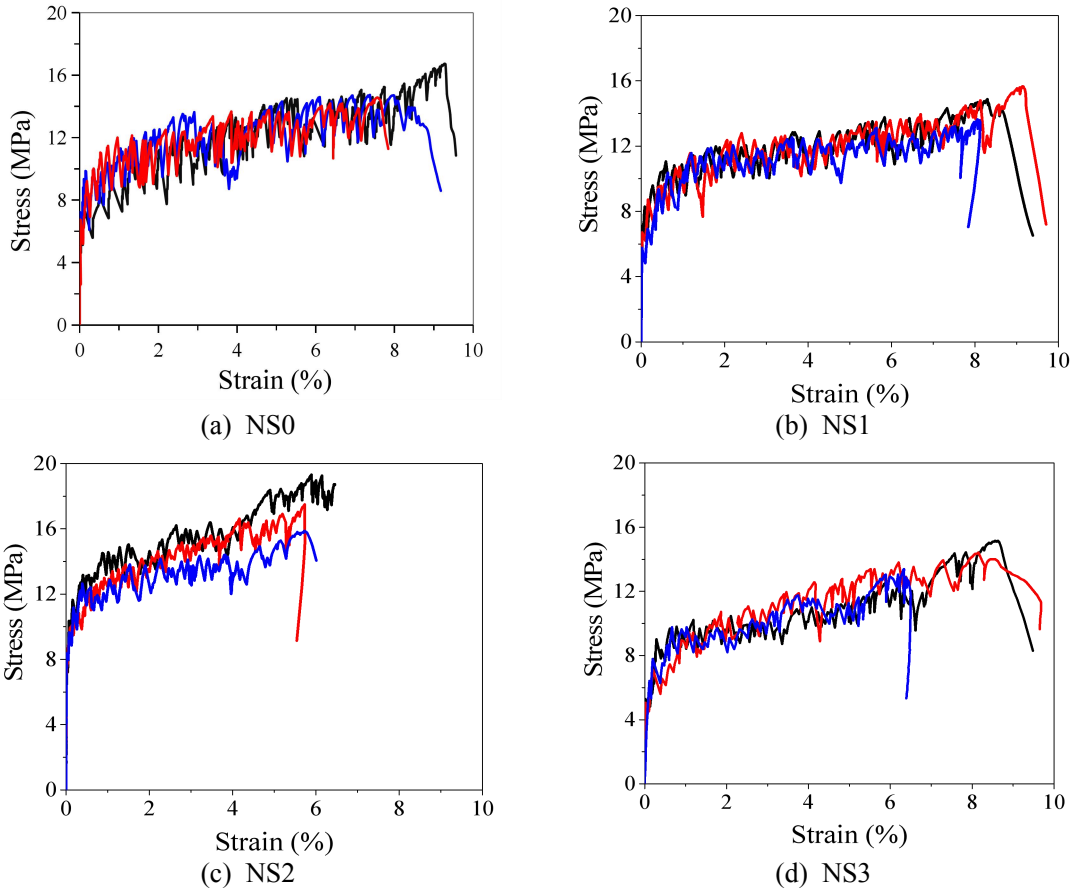

Fig. 11 Tensile relationship of HS-SHCC with different NS dosages at 28d

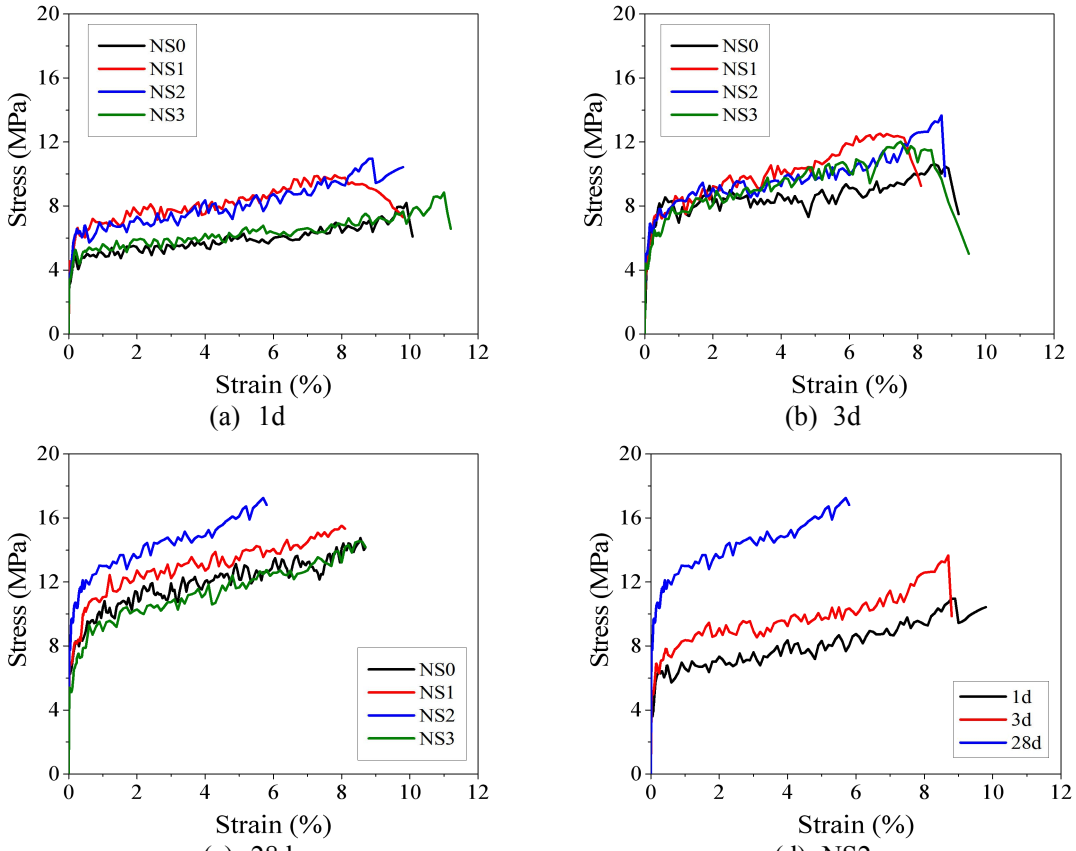

(a) 1d (b) 3d

(c) 28d (d) NS2

Fig. 12 Average tensile relationship of HS-SHCC at 1d, 3d and 28d

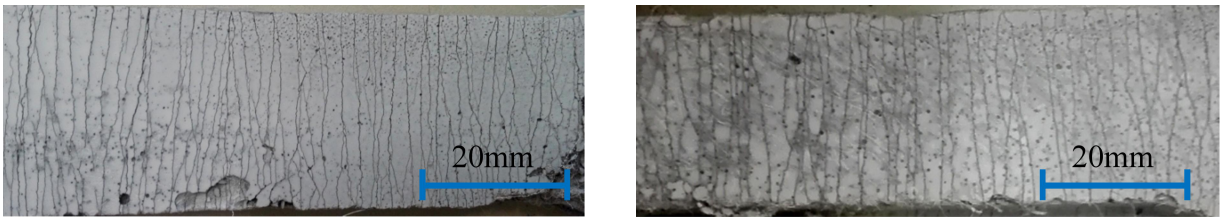

(a) NS2-3d (b) NS2-28d

Fig. 13 Crack patterns of NS2 under direct tension at different ages

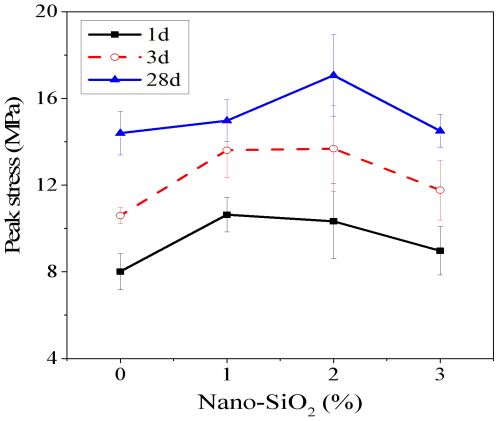

(a) Peak stress

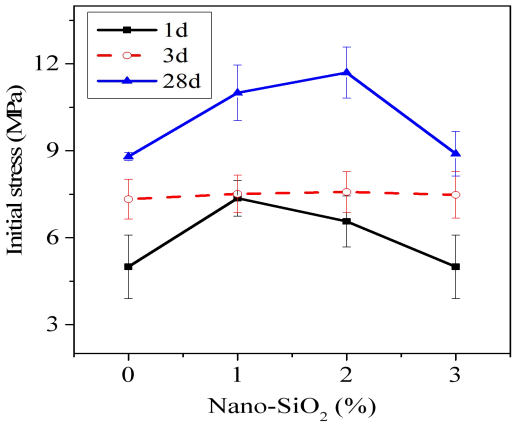

(b) Initial cracking stress

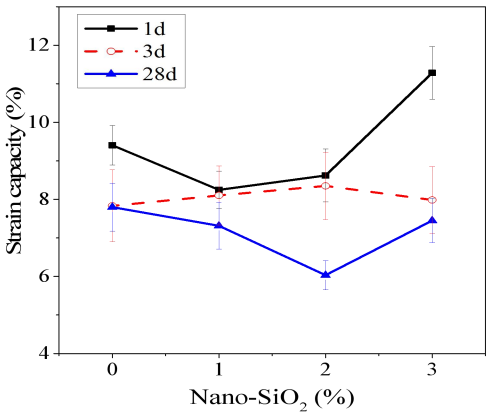

(c) Strain capacity

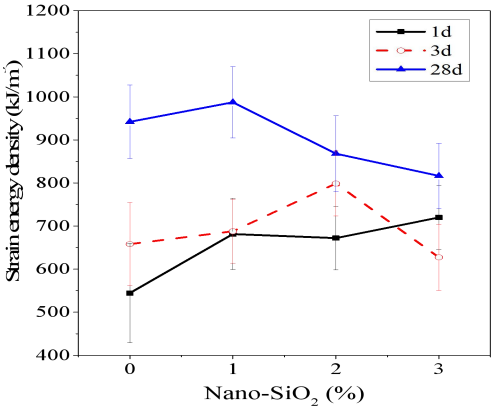

(d) Strain energy density

Fig. 14 Tensile parameters of NS-modified HS-SHCC

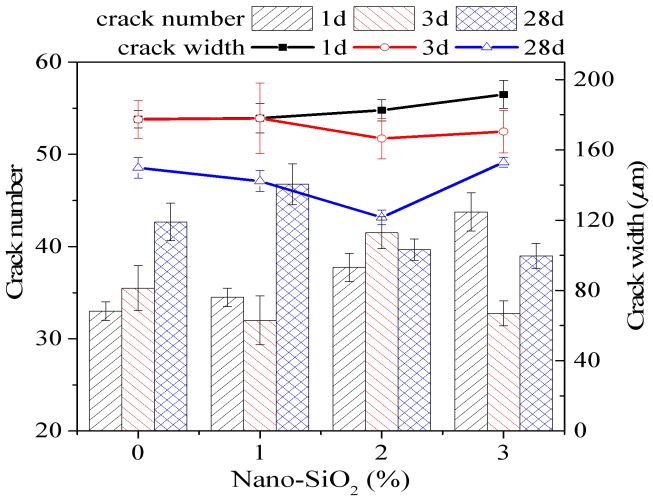

Fig. 15 Crack pattern parameter of HS-SHCC

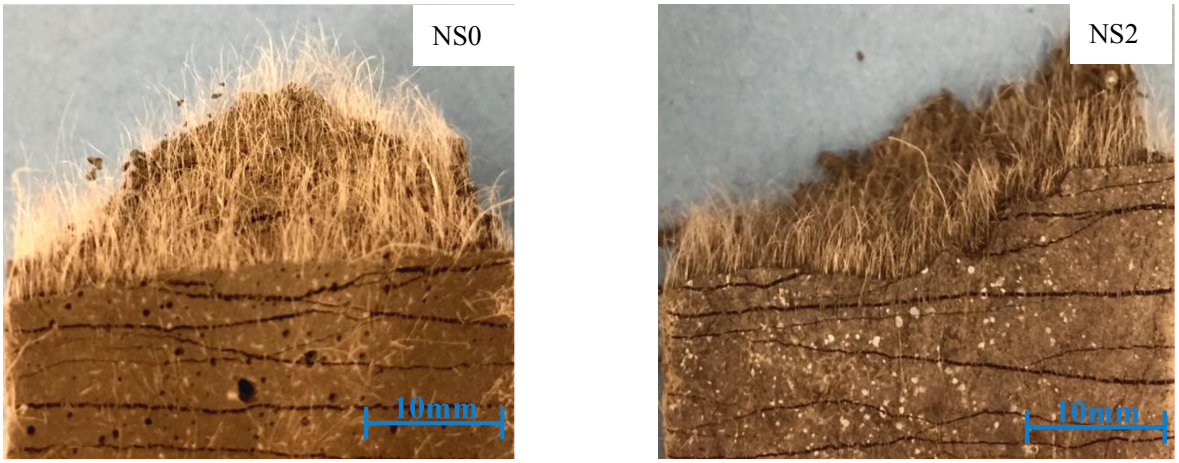

(a) NS0 (b) NS2

Fig. 16 Comparison of fracture surfaces of NS0 and NS2

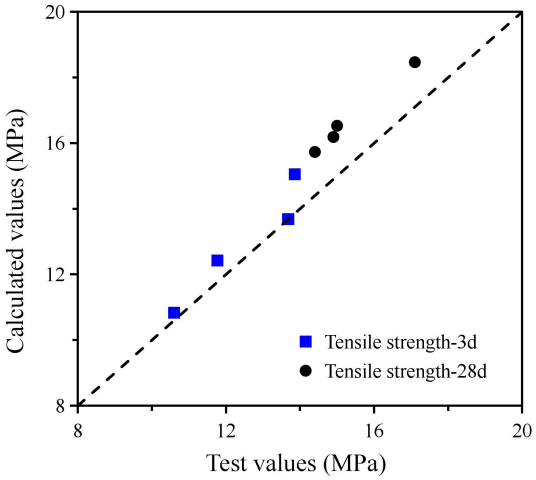

Fig. 17 Comparison of experimental and analytical tensile strength values

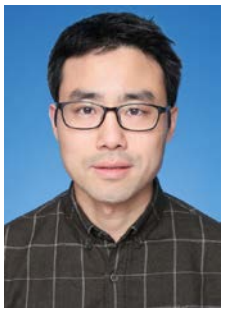

Kequan Yu

Weihao Mao

Yao Ding

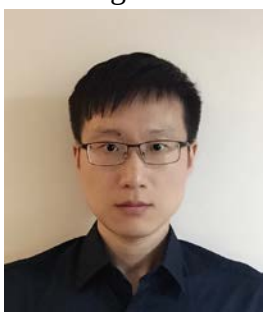

Shuo Zhang